

Article

A Novel Digital Control Method of a Single-Phase Grid-Connected Inverter Based on a Virtual Closed-Loop Circuit and Complex Vector Representation

Kun Xie ^{1,2,*}, Gangyi Hu ², Hong Yi ¹, Zhibi Lyu ³ and Yangxiao Xiang ³

¹ State Key Laboratory of Ocean Engineering, Shanghai Jiao Tong University, Shanghai 200240, China; yihong@sjtu.edu.cn

² China Ship Development and Design Center, Wuhan 430064, China; zjuxiekun@163.com

³ State Key Laboratory of Advanced Electromagnetic Engineering and Technology, Huazhong University of Science and Technology, Wuhan 430074, China; lyuzhibi@whu.edu.cn (Z.L.); xyxhhsx@163.com (Y.X.)

* Correspondence: xiekun@sjtu.edu.cn

Received: 26 October 2017; Accepted: 30 November 2017; Published: 6 December 2017

Abstract: With the rapid development of renewable energy generation, single-phase grid-connected inverters have been widely applied in modern power systems. Since the power output of the renewable sources is continuously changing, independent active/reactive power control and a rapid current tracking performance is supposed to be achieved in a single-phase grid-connected inverter. However, the poor orthogonal-axis-constructing strategy and the ineffective decoupling in some widely-used controllers have severely weakened the dynamic performance of the single-phase inverter. To deal with the challenges above, this study proposes a comprehensive control strategy for current control in a single-phase grid-connected inverter. In the proposed control strategy, a virtual closed-loop is constructed to improve the dynamic performance and realize independent power control under a synchronous frame. Then, complex vector theory is used to model the virtual closed-loop based single-phase inverter, and a novel digital controller is designed based on zero-pole cancellation and minimum beat control to completely decouple the active/reactive components and achieve a supreme current tracking performance. Experimental results are shown to validate the feasibility of the proposed current controller.

Keywords: single-phase inverter; virtual closed-loop circuit; current decoupling control; complex vector; discrete domain

1. Introduction

With the raising demand of high-efficiency and environmental-friendly electric power supply, micro-grids have been widely applied as a new kind of distribution network structure, which significantly facilitates access for renewable distributed generation (DG) such as photo-voltaic plants and wind turbines [1–7]. Among various connecting methods, the single-phase grid-connected inverter is one of the commonly used interfaces for DGs [8,9]. Due to the continuously-changing power output of the renewable resources, a better control performance is expected for the single-phase grid-connected inverter [10,11]. In particular, the single-phase grid-connected inverter should achieve independent active/reactive power control, and has the rapid dynamic performance to track the changing output power of the renewable sources.

In the past several decades, various control techniques have been proposed to improve the performance of the single-phase inverter, among which Proportional-Integral (PI) control is most widely applied in the single-phase inverter, due to its good steady and dynamic performance. To realize

the independent control of the active/reactive powers and achieve the zero steady-state error, the dq synchronous reference frame is applied in the single-phase inverter [12]. However, there are two main problems to be addressed: one is constructing the orthogonal axis, and the other is the coupling with the synchronous frame. A poor orthogonal-axis-constructing strategy and ineffective decoupling would weaken the dynamic performance of the whole system.

Generally, the orthogonal axis is constructed by delaying the real axis by 90° to realize PI control under the synchronous frame. However, any disturbance in the system may reflect in orthogonal axis after $1/4$ fundamental cycle, which has a severe effect on the dynamic response of the system [13]. In [14], the orthogonal axis is constructed by the Hilbert transform. However, the Hilbert transform can only be applied to narrow-band signals, so in many situations, the actual signal cannot meet the requirements of Hilbert transform because of the noise. In [15], an all-pass filter is applied to form the orthogonal axis, but the design of the all-pass filter is very complicated considering the stability problems, and it would waste significant computation consumption.

When the PI control is applied to the inverters in the synchronous reference frame, the current coupling exists between d-axis and q-axis [16–20]. At present, many scholars have conducted research to deal with the coupling issue. In [16], the current coupling effect was reduced, when applying the large forward channel gain to the close-loop control. However, in practical application, the gain of the controller cannot be set as a very large value, since a large gain would threaten the stability of the system. The inductor current state feedback (ICSF) is the most commonly used method to decouple the dq axis [17]. However, ICSF cannot eliminate the coupling caused by the digital delay. A one-step predicting scheme (PRE-ICSF) was proposed to deal with the coupling issue caused by the digital delay [18]. In this method, the predicted current is used to generate the decoupling term. However, when parameter deviation occurs, the decoupling effect would be significantly influenced in ICSF and PRE-ICSF. To overcome the shortcoming, a complex vector-based controller is proposed, because it has a robust decoupling performance against the digital delay and inductance parameter deviation [19,20]. However, the application of the complex vector into a single-phase situation has not been discussed.

In order to enhance the dynamic active/reactive power tracking performance of the single-phase grid-connected inverter, a novel current control strategy is proposed to deal with shortcomings of the previous methods. For the proposed control strategy, two main functions are supposed to be realized. An orthogonal axis constructing method, which has a rapid dynamic response to the disturbance in the system, is brought out to achieve independent active/reactive power control in a single-phase inverter. Additionally, the coupling issue in the single-phase inverter is discussed and an improved complex-vector based controller, which is applied in the single-phase situation, is designed to realize precise decoupling of the system.

The paper is organized as follows: in Section 2, a virtual closed-loop is constructed for the single-phase inverter; in Section 3, the single-phase inverter with a virtual closed-loop is modeled under complex vector theory; Section 4 further designs the complex vector-based controller in the discrete domain; Section 5 illustrates the experimental results to verify the effectiveness of the proposed controller; and conclusions are drawn in Section 6.

2. Virtual Closed-Loop Construction

The topology of a single-phase rectifier is shown as Figure 1. v_{gs} refers to the AC voltage, i_s refers to the AC current, L and r are the total value of the inductance and resistor at the AC side, and V_{dc} is the voltage of the DC side.

The mathematic model of the single-phase inverter can be expressed as:

$$L \frac{di_s}{dt} + ri_s = v_{is} - v_{gs} \quad (1)$$

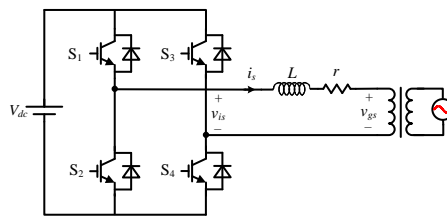


Figure 1. Single-phase grid-connected full bridge voltage source inverter.

In order to achieve PI control in synchronous coordinates, a virtual circuit, which is realized in the controller, is constructed as shown in Figure 2.

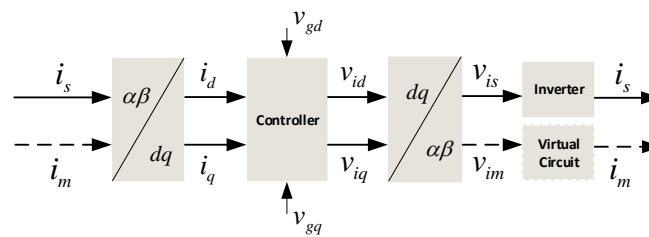


Figure 2. Improved control diagram for a single-phase inverter.

In Figure 2, component i_s represents the AC current sampled in the real circuit, v_{is} and v_{im} are the modulation signals generated from the current controller. The modulation signal of the orthogonal axis v_{im} is utilized to calculate the virtual AC current as:

$$i_m(s) = \frac{v_{im} - v_{gm}}{Ls + r} \tag{2}$$

The values of the virtual inductor and virtual resistor are equal to the real ones (L and r). i_m is orthogonal to i_s and can be used to form the virtual closed-loop. The introduction of the virtual closed-loop can rapidly respond to the change of the real component and greatly improve the dynamic performance of the single-phase inverter.

The introduction of the virtual closed-loop changes the transfer function of the controlled plant. The mathematic model of the virtual circuit is described as:

$$L \frac{di_m}{dt} + ri_m = v_{im} - v_{gm} \tag{3}$$

Transforming Equations (1) and (3) into the dq synchronous reference frame, the mathematical model of the newly-constructed controlled plant can be deduced as:

$$L \frac{di_d}{dt} + ri_d - \omega Li_q = v_{id} - v_{gd} \tag{4}$$

$$L \frac{di_q}{dt} + ri_q + \omega Li_d = v_{iq} - v_{gq} \tag{5}$$

Obviously, the introduction of the virtual closed-loop circuit makes the model of the single-phase inverter the same as the three-phase inverter. They share the same dynamic characteristics, theoretically. However, the virtual closed-loop also brings the coupling problem for the system, which will severely influence the accurate tracking performance of the single-phase system. Therefore, the current controller should be further improved to realize independent control of the active/reactive power.

3. Discrete Model of the Inverter Considering the Influence of Delay Based on Complex Vectors

The mathematical model of the polyphasic system can be either expressed in scalar or complex vector forms. Generally, the scalar is most commonly used for the system modeling as analyzed in the last section, and the model of the single-phase inverter with the virtual closed-loop can be regarded as a double-input dual-output second-order system. In order to further study the coupling issue, a complex vector can be applied to reduce the order of the system. The complex vector is defined as:

$$f_{\alpha\beta} = f_{\alpha} + jf_{\beta} \quad (6)$$

where f_{α} and f_{β} represent a pair of orthogonal quantities. Therefore, the virtual closed-loop based inverter model will become a single-input single-output first-order system as:

$$i_{\alpha\beta}(s) = \frac{1}{Ls + r} v_{i\alpha\beta} - \frac{1}{Ls + r} v_{g\alpha\beta} \quad (7)$$

where $i_{\alpha\beta} = i_s + ji_m$, $v_{i\alpha\beta} = v_{is} + jv_{im}$, $v_{g\alpha\beta} = v_{gs} + jv_{gm}$. Regarding the grid voltage as a perturbation, the transfer function of the controlled-plant in the stationary coordinate system could be obtained by rewriting Equation (7) in the form of the voltage input and current output:

$$G_{\alpha\beta}(s) = \frac{i_{\alpha\beta}(s)}{v_{i\alpha\beta}(s)} = \frac{1}{Ls + r} \quad (8)$$

Transforming Equation (8) into the synchronous coordinate system, in which the Laplace operator s is replaced by $s + j\omega$, the mathematical model of the controlled plant in the dq synchronous reference frame can be obtained:

$$G_{dq}(s) = \frac{i_{dq}(s)}{v_{idq}(s)} = \frac{1}{Ls + r + j\omega L} \quad (9)$$

To analyze the degree of system coupling, the symmetry degree of the closed-loop transfer function around 0 Hz can be used as an index to measure the coupling degree of closed-loop system, which can be mathematically expressed as:

$$|\Delta H| = \left| \frac{H(j\omega) - H^*(-j\omega)}{2j} \right| \quad (10)$$

For a fully-decoupled system, $|\Delta H|$ is equal to 0 in the whole frequency range, i.e., $H(j\omega) = H^*(-j\omega)$. The frequency response characteristics of its closed-loop transfer function should be strictly symmetric around 0 Hz (even symmetrical for the amplitude-frequency characteristics, odd symmetry for the phase-frequency characteristics).

In the complex vector based model, the coupling item is represented as the imaginary term, which makes the frequency characteristic of the controlled plants no longer symmetrical around 0 Hz, as in the stationary reference frame (shown in Figure 3).

Generally, a synchronous frame PI regulator is chosen as the current controller and the block diagram is shown as Figure 4. In the design of PI controller, K_p/K_i is typically selected equal to r/L , which optimizes the performance of the system by introducing a zero point to cancel the pole of the controlled plant and turning the closed-loop transfer function of the whole system into an inertia link. The bandwidth of the controller is adjusted by tuning the value of K_p . $\omega\hat{L}$ denotes the decoupling item.

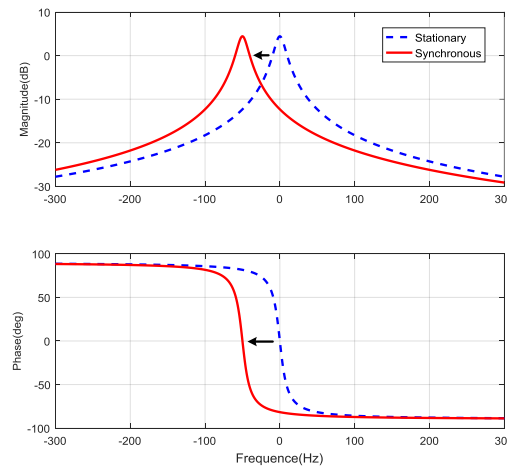


Figure 3. The frequency-response function (FRF) of the controlled object in the rotating coordinate system and the stationary coordinate system.

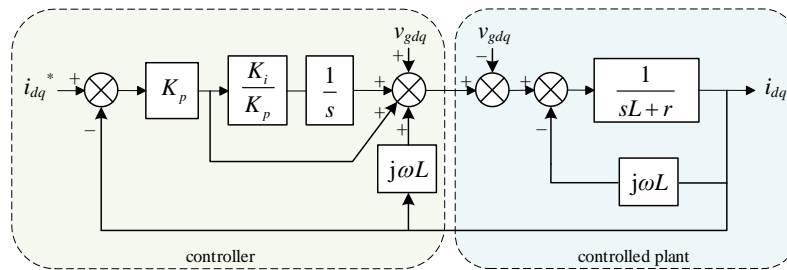


Figure 4. Complex vector block diagram of the inverter with a cross-coupling decoupling synchronous frame PI current controller, shown in the synchronous reference frame.

The closed-loop transfer function of the PI current control system in synchronous frame can be deduced as:

$$H_{clo}(s) = \frac{K_p s + K_i}{Ls^2 + [K_p + r + j\omega(L - \hat{L})]s + K_i} \tag{11}$$

where \hat{L} is the measured value of the AC inductor, and L is used as the setting value in the controller. When the sampling frequency is f_s , the sampling period is $T_s = 1/f_s$. Equation (11) can be discretized as:

$$H_{clo}(z) = \frac{(K_p + K_i T_s) T_s z^2 - K_p T_s z}{A z^2 - B z + L} \tag{12}$$

where:

$$A = L + (K_p + K_i T_s + r + j\omega L - j\omega \hat{L}) T_s \tag{13}$$

$$B = 2L + (K_p T_s + r + j\omega L - j\omega \hat{L}) T_s \tag{14}$$

According to Equation (12), the frequency characteristics with a current state feedback decouple PI controller for variations in \hat{L} are shown in the synchronous reference frame. As can be seen from Figure 5, the frequency response waveform becomes asymmetric when the inductor is measured with errors. The waveform is distorted near 0 Hz (corresponds to the synchronous frequency in the stationary reference frame) and the resonant peak appears. In this case, the decoupling of the system will no longer be complete, which means the active current control and the reactive current control interact with each other, and the system’s control performance deteriorates.

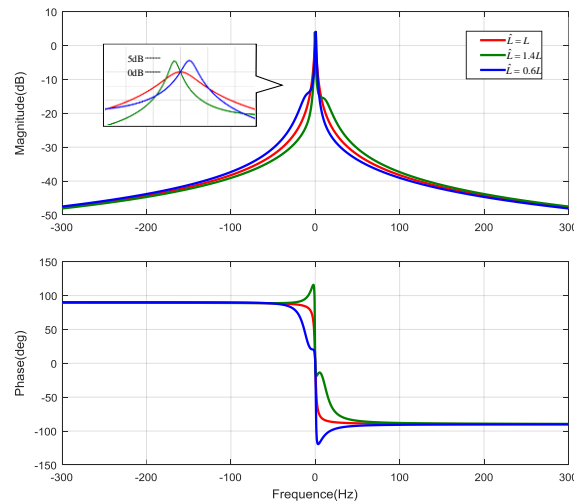


Figure 5. Complex vector FRF for variations in \hat{L} of the inverter with a cross-coupling decoupling synchronous frame PI current controller, shown in the synchronous reference frame.

4. Complex Vector-Based Controller

In order to achieve complete independent control of the active/reactive power, a discrete model of the grid-connected inverter is established by using the complex vector, and the controller is designed accordingly.

4.1. Discrete Model of the Complex Vector-Based Inverter

Since the modulating signals are updated at the beginning of every cycle, the controlled plant could be discretized by using a zero-order holder as:

$$T(s) = \frac{1 - e^{-sT_s}}{s} \quad (15)$$

Thus, the complex vector based discrete model of the single-phase inverter with a virtual closed-loop can be deduced as:

$$G_{\alpha\beta}(z) = Z(T(s)G_{\alpha\beta}(s)) = \frac{1 - e^{-\frac{r}{L}T}}{(z - e^{-\frac{r}{L}T})r} \quad (16)$$

Equation (16) can also be expressed as a differential equation as:

$$i_{\alpha\beta}(k+1) = i_{\alpha\beta}(k)e^{-\frac{r}{L}T_s} + v_{\alpha\beta}(k) \frac{1 - e^{-\frac{r}{L}T_s}}{r} \quad (17)$$

According to the principle of coordinate transformation, the relationship between the stationary coordinate system and the synchronous rotation coordinate system is given by:

$$f_{\alpha\beta}(k)e^{-j\theta(k)} = f_{dq}(k) \quad (18)$$

In the $k+1$ th cycle, according to the equation $e^{-j(\theta(k+1))} = e^{-j(\theta(k)+\omega T_s)}$, the differential equation in the synchronous reference frame can be calculated as:

$$i_{\alpha\beta}(k+1)e^{-j(\theta(k+1))} = i_{\alpha\beta}(k)e^{-\frac{r}{L}T_s}e^{-j(\theta(k)+\omega T_s)} + v_{\alpha\beta}(k) \frac{1 - e^{-\frac{r}{L}T_s}}{r}e^{-j(\theta(k)+\omega T_s)} \quad (19)$$

Using Equations (18) and (19), the discrete transfer function of the controlled plant in the synchronous dq reference frame can be preliminarily obtained as:

$$G_{dq}(z) = \frac{1 - e^{-\frac{r}{L}T_s}}{(ze^{j\omega T_s} - e^{-\frac{r}{L}T_s})r} \tag{20}$$

Consider the intrinsic one-beat digital delay in the digital signal processor (DSP), where the modulation quantities $D(k)$ calculated in the k th cycle will not be immediately applied to control the inverter until the beginning of the $k + 1$ th cycle. The transfer function of the digital delay in the stationary reference frame is z^{-1} , and it can be rewritten in the synchronous dq reference frame as:

$$D(z) = (ze^{j\omega T_s})^{-1} \tag{21}$$

Equation (21) can be expressed in the form of the differential equation as:

$$u_{\alpha\beta}(k) = u_{\alpha\beta}(k - 1)(\cos(\omega T_s) - j \sin(\omega T_s)) \tag{22}$$

Therefore, the discrete transfer function of the controlled plant in synchronous dq reference frame can be ultimately obtained considering the one beat digital delay:

$$G_{dq}(z) = D(z)G_{dq}(z) = \frac{1 - e^{-\frac{r}{L}T_s}}{ze^{j\omega T_s}(ze^{j\omega T_s} - e^{-\frac{r}{L}T_s})r} \tag{23}$$

According to Equation (23), the expression of the main pole is:

$$p_1 = e^{-\frac{r}{L}T_s - j\omega T} = e^{-\frac{r}{L}T_s}(\cos(\omega T_s) - j \sin(\omega T_s)) \tag{24}$$

Clearly, the main pole p_1 changes with the sampling frequency, which is exhibited in Figure 6. Due to the small value of the sampling period, these poles are close to the edge of the z-plane unit circle, which may cause the system to oscillate. Additionally, the main pole will be farther away from the real axis with the decreasing of the sampling frequency, and the dq axis current coupling becomes more serious.

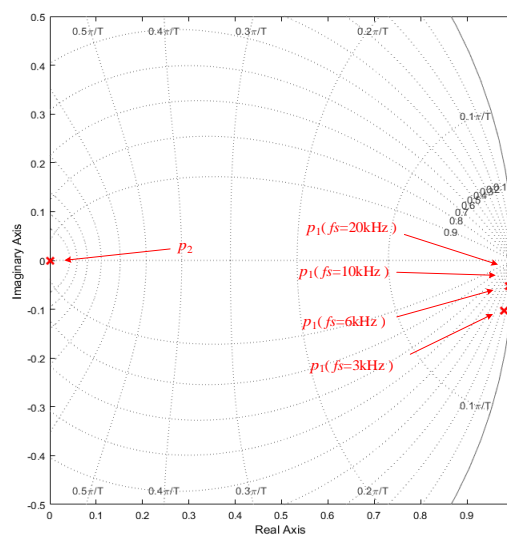


Figure 6. The location of the poles for the closed-loop transfer function in Equation (23).

From Equation (23) and Figure 6, it can also be seen that the time delay of the control system introduces an additional pole (p_2) into the discrete model of the inverter. The time delay will worsen the dq axis current cross-coupling, and further deteriorate the transient performance of the current loop.

4.2. Controller Design

In order to completely decouple the system, the controller can be designed by introducing the complex zero to cancel the complex pole in the controlled plant. Additionally, since there exist no zeros and poles outside of the unit circle in the discrete model of the controlled plant, the system satisfies the designing requirement of minimum beat control. Therefore, the controller proposed in this paper is expressed as Equation (25), whose block diagram is shown as Figure 7.

$$C_{dq}(z) = \frac{Ke^{j\omega T_s} r (e^{j\omega T_s} - e^{-\frac{r}{L} T_s} z^{-1})}{(1 - e^{-\frac{r}{L} T_s})(1 - z^{-1})(1 + z^{-1})} \quad (25)$$

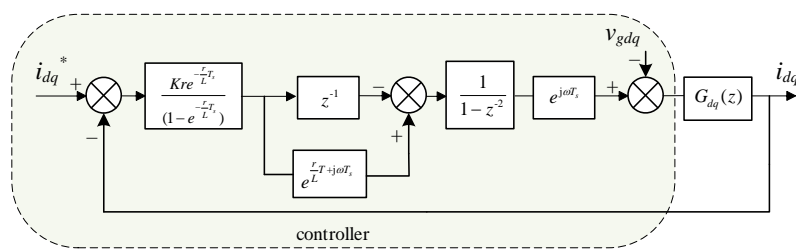


Figure 7. Complex vector block diagram of the inverter with the proposed control strategy, shown in the synchronous reference frame.

If there is no deviation between the setting inductance value and the actual inductance value, the closed-loop transfer function of the current control system in the synchronous dq reference frame can be calculated as:

$$H_{clo}(z) = \frac{G_{dq}(z)C_{dq}(z)}{1 + G_{dq}(z)C_{dq}(z)} = \frac{K}{z^2 + K - 1} \quad (26)$$

It can be seen that the AC current will reach the given reference value after several finite steps. Especially when K equals 1, Equation (26) can be simplified as $H_{clo}(z) = z^{-2}$, which indicates that it will take only two steps for the AC current to reach the given reference value without ripples, theoretically. Although the dynamic response could not achieve such a fast response time in practice for various factors, the proposed controller still indicates a better dynamic performance compared with the traditional PI regulator.

If the setting value of inductance \hat{L} is biased with the actual situation, the open-loop and closed-loop transfer functions become:

$$H_{open}(z) = \frac{(1 - e^{-\frac{r}{\hat{L}} T_s})}{(1 - e^{-\frac{r}{L} T_s})} \frac{(ze^{j\omega T_s} - e^{-\frac{r}{\hat{L}} T_s})}{(ze^{j\omega T_s} - e^{-\frac{r}{L} T_s})(z^2 - 1)} = \frac{K'(ze^{j\omega T_s} - e^{-\frac{r}{\hat{L}} T_s})}{(ze^{j\omega T_s} - e^{-\frac{r}{L} T_s})(z^2 - 1)} \quad (27)$$

$$H_{clo}(z) = \frac{K'(ze^{j\omega T_s} - e^{-\frac{r}{\hat{L}} T_s})}{(ze^{j\omega T_s} - e^{-\frac{r}{L} T_s})(z^2 - 1) \left[1 + \frac{K'(ze^{j\omega T_s} - e^{-\frac{r}{\hat{L}} T_s})}{(ze^{j\omega T_s} - e^{-\frac{r}{L} T_s})(z^2 - 1)} \right]} \quad (28)$$

From Equation (27), it seems that the inaccurate inductance value will also influence the completeness of the zero-pole cancellation as well as the gain of the open-loop transfer function. However, due to the small value of the switching period T_s and resistance r , the inductance bias will have little influence on the decoupling effect. Figure 8 shows the frequency characteristics of

the closed-loop transfer function when applying the proposed control scheme. It can be clearly seen that when the parameter deviation occurs, the frequency response characteristics basically maintain symmetry at 0 Hz, which indicates that the proposed controller can effectively decouple the dq axis under the synchronous frequency when parameter deviation occurs. Furthermore, the amplitude at 0 Hz stays at 1 dB, which indicates that zero-steady-error will be achieved. Therefore, the proposed control strategy can effectively eliminate the influence of the inaccurate inductance value and greatly improve the tracking performance of the single-phase grid-connected inverter.

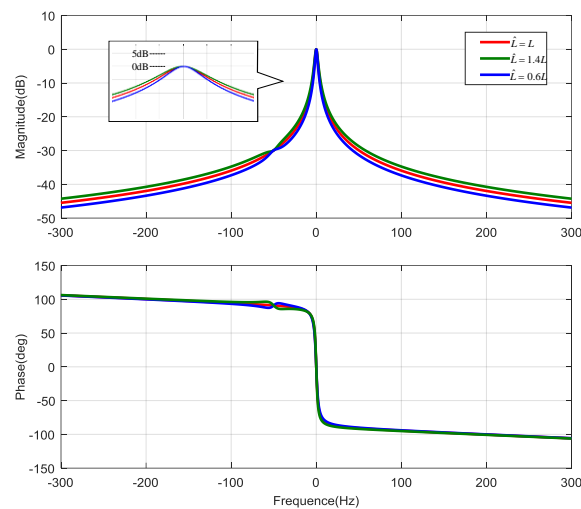


Figure 8. Complex vector FRF for variations in \hat{L} of the inverter with a cross-coupling decoupling synchronous frame PI current controller, shown in the synchronous reference frame.

5. Experimental Results

To verify the performance of the proposed current controller, laboratory experiments were carried out on a single-phase grid-connected inverter as shown in Figure 9. The pertinent parameters related to the inverter are shown in Table 1. The system is connected to the grid through a transformer. The current probe is used to measure the AC current i_s . To study the dynamic process of the system in a detailed manner, I_d and I_q are converted to analog voltage signals by the digital-to-analog converter (DAC) module and displayed on the oscilloscope.

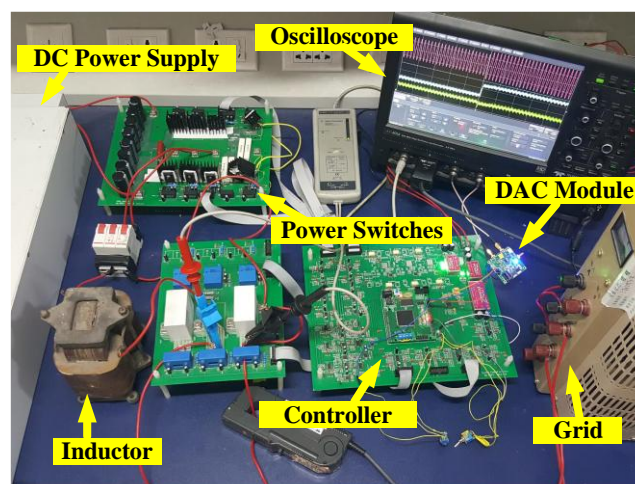


Figure 9. Photograph of the experimental setup.

Table 1. Parameters and components of the grid-connected inverter.

Parameter	Variable	Value
Grid Voltage	v_g	110 V
Grid Frequency	f_0	50 Hz
Grid-Tie Inductor	L	13.6 mH
Resistance of the inductor	r	0.6 Ω
Switching Frequency	f_s	12 kHz
DC-Link Voltage	V_{dc}	200 V
Components		Part Number
IGBTs(S ₁ –S ₄)		IKW40T120
Digital Signal Controller		TMS320F28335
DC power supply		PSI81500-30
Current Probe		CP150
Oscilloscope		HDO4054

Figure 10 shows the block diagram of the proposed control strategy. The block with the buff background is the current controller which is realized in DSP. The grid voltage v_{gs} and the AC current i_s are sampled into the DSP through the hall sensors. The virtual closed-loop is constructed according to the digital calculation described in Section 2, and the orthogonal virtual grid voltage v_{gm} , as well as the virtual AC current i_m is then obtained. Then these four quantities are applied to form the complex vector-based current loop. Finally, modulating signals are generated to control the single-phase inverter.

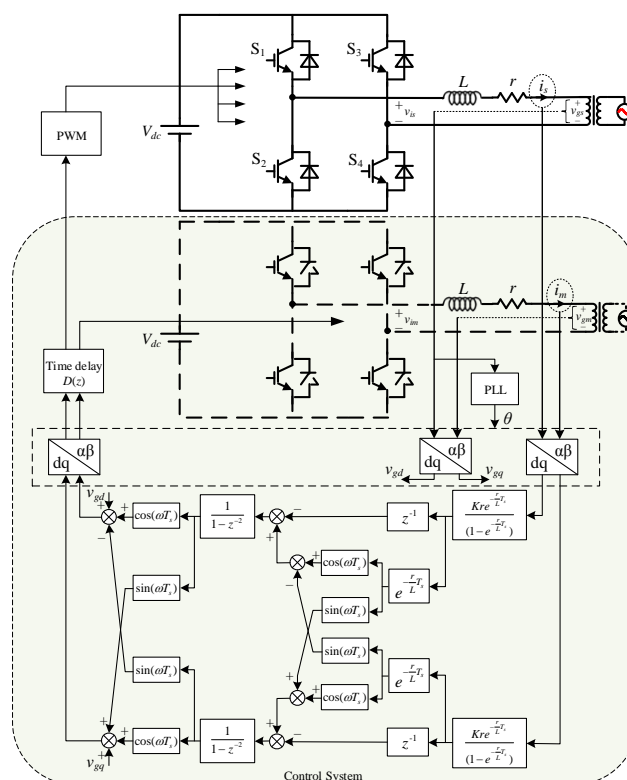


Figure 10. Block diagram of the grid-connected inverter with the proposed control strategy.

Figure 11 shows the dynamic waveform of current controller with the traditional 90°-delay method as introduced in [13]. The given current reference mutates at the middle of the figure, where the d-axis current reference is changed from 5 A to 8 A, and the q-axis current reference remains at 5 A. Obviously, it takes a long time for the controller to react to the disturbance, and this method also

introduces a very large fluctuation to the system. Figures 12–14 show the dynamic waveform based on the virtual closed-loop, and there is no large fluctuation when the current reference changes.

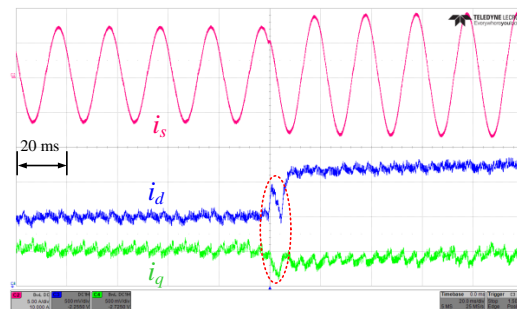


Figure 11. Experimental results with the proposed control strategy while the virtual closed-loop circuit is removed.

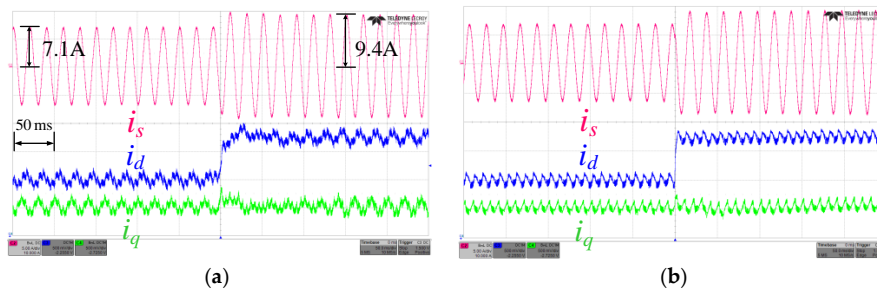


Figure 12. Experimental results for the inductance current i_s , the d-axis current i_d , the q-axis current i_q when $\hat{L} = L$. (a) ICSF-based PI control; and (b) the proposed complex vector based control.

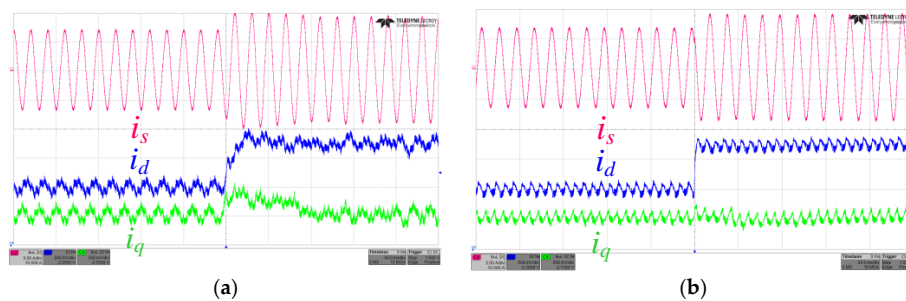


Figure 13. Experimental results for the inductance current i_s , the d-axis current i_d , the q-axis current i_q when $\hat{L} = 1.4L$. (a) ICSF-based PI control; and (b) the proposed complex vector based control.

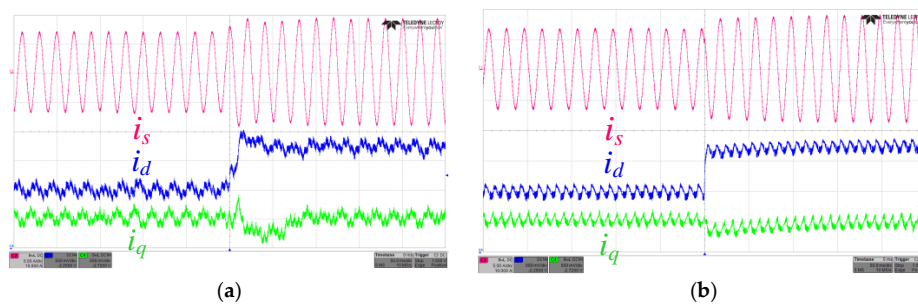


Figure 14. Experimental results for the inductance current i_s , the d-axis current i_d , the q-axis current i_q when $\hat{L} = 0.6L$. (a) ICSF based PI control; and (b) the proposed complex vector based control.

Figures 12–14 compare the decoupling effect of the traditional ICSF-based PI controller and the proposed controller when parameter deviation occurs. The experimental results show that both of the two control modes can achieve high steady accuracy and low distortion degrees of the output waveform. Comparing Figure 12a, Figure 13a, and Figure 14a, it can be seen that the deviation of the inductance will severely deteriorate the dynamic performance of the ICSF-based controller. For the proposed controller (by comparing Figure 12b, Figure 13b, and Figure 14b), the parameter deviation will have little influence on the decoupling effect. Additionally, according to Figure 12a,b, the proposed method shows a better dynamic performance than the traditional ICSF-based PI controller.

Figure 15 shows the details of the step responses with the proposed control strategy. t_d is the inherent time delay of the DAC module. t_0 denotes the step response time of the d-axis current. It can be seen that it takes several finite steps ($t_0 \approx 583 \mu\text{s}$) to reach the reference value, rather than only a two-step response time, theoretically. These results all reveal that the proposed method has low parameter sensitivity and improves the transient state performance of the current control. Moreover, the computational cost of these two control strategies in the DSP (TMS320F28335, a member of the TMS320C28x/Delfino™ DSC/MCU generation, is produced by Texas Instruments, Shanghai, China) has been tested. The traditional control method costs $25.6 \mu\text{s}$ during one switching period, while the new control method costs $26.8 \mu\text{s}$ during one switching period (with the DSP controller clocked at 150 MHz). Therefore, the proposed control strategy would not add to the computational consumption compared with traditional methods, and is also suitable for high-frequency applications.

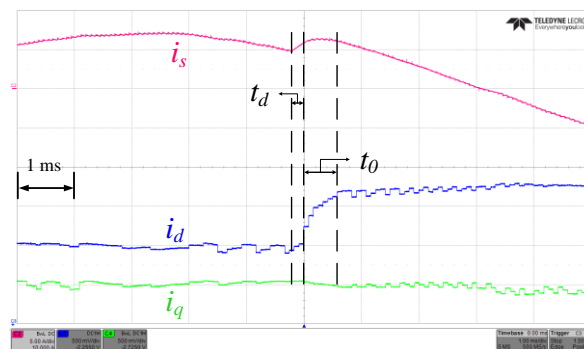


Figure 15. Details of the step responses with the proposed control strategy.

6. Conclusions

This paper proposes a comprehensive control scheme for a single-phase grid-connected inverter. Two main procedures have been conducted to enhance the dynamic performance of the single-phase inverter. Firstly, a virtual closed-loop is constructed to realize PI control under a synchronous dq frame, which effectively achieves the independent control of active/reactive power, and significantly improves the dynamic performance by converting a single-phase inverter into a three-phase inverter model. Then, based on complex vector theory, a novel digital controller is designed to completely decouple the active/reactive power and achieve an optimal dynamic performance. The proposed control scheme is experimentally proved to have superior current tracking performance.

Acknowledgments: This work was supported by the State Key Laboratory of Ocean Engineering from Shanghai Jiao Tong University, the China Ship Development and Design Center, and the State Key Laboratory of Advanced Electromagnetic Engineering and Technology from Huazhong University of Science and Technology.

Author Contributions: All authors contributed to this work by collaboration. The authors contributed equally to the theoretical analysis, modeling, simulation, experiments, and manuscript preparation. All authors revised and approved for the publication.

Conflicts of Interest: The authors declare no conflict of interest.

Abbreviations

V_{dc}	DC-link voltage
L	Grid-tie inductor
r	Resistance of the inductor
i	Grid-connected current
v_{is}	Port voltage of the inverter
v_{gs}	Grid voltage of the AC side
i_m	Virtual grid-connected current
v_{im}	Port voltage of the inverter in the virtual closed-loop circuit
v_{gm}	Virtual grid voltage of the AC side
\hat{L}	The setting value of the inductance
ω	Angular frequency of the grid voltage
T_s	Sampling period
$G(s)$	The transfer function of the controlled plant
$C(s)$	The transfer function of the controller
$H(s)$	The transfer function of the whole system

References

1. Marzband, M.; Parhizi, N.; Savaghebi, M.; Guerrero, J.M. Distributed Smart Decision-Making for a Multimicrogrid System Based on a Hierarchical Interactive Architecture. *IEEE Trans. Energy Convers.* **2016**, *31*, 637–648. [[CrossRef](#)]
2. Valinejad, J.; Marzband, M.; Akorede, M.F.; Barforoshi, T.; Jovanović, M. Generation expansion planning in electricity market considering uncertainty in load demand and presence of strategic GENCOs. *Electr. Power Syst. Res.* **2017**, *152*, 92–104. [[CrossRef](#)]
3. Marzband, M.; Azarnejadian, F.; Savaghebi, M.; Guerrero, J.M. An Optimal Energy Management System for Islanded Microgrids Based on Multiperiod Artificial Bee Colony Combined With Markov Chain. *IEEE Syst. J.* **2017**, *11*, 1712–1722. [[CrossRef](#)]
4. Mortezaei, A.; Simões, M.G.; Busarello, T.D.C. A multi task microgrid inverter based instantaneous Power Theory in islanded and grid-connected modes. In Proceedings of the 2015 IEEE Power & Energy Society General Meeting, Denver, CO, USA, 26–30 July 2015; pp. 1–5.
5. Marzband, M.; Ardeshiri, R.R.; Moafi, M.; Uppal, H. Distributed generation for economic benefit maximization through coalition formation-based game theory concept. *Int. Trans. Electr. Energy Syst.* **2017**, *27*, e2313. [[CrossRef](#)]
6. Marzband, M.; Moghaddam, M.M.; Akorede, M.F.; Khomeyrani, G. Adaptive load shedding scheme for frequency stability enhancement in microgrids. *Electr. Power Syst. Res.* **2016**, *140*, 78–86. [[CrossRef](#)]
7. Marzband, M.; Ghazimirsaeid, S.S.; Uppal, H.; Fernando, T. A real-time evaluation of energy management systems for smart hybrid home Microgrids. *Electr. Power Syst. Res.* **2017**, *143*, 624–633. [[CrossRef](#)]
8. Yang, Y.; Koutroulis, E.; Sangwongwanich, A.; Blaabjerg, F. Pursuing Photovoltaic Cost-Effectiveness: Absolute Active Power Control Offers Hope in Single-Phase PV Systems. *IEEE Ind. Appl. Mag.* **2017**, *23*, 40–49. [[CrossRef](#)]
9. Kadam, S.; Bletterie, B. Balancing the grid with single-phase PV-installations. In Proceedings of the 2017 IEEE 26th International Symposium on Industrial Electronics (ISIE), Edinburgh, UK, 19–21 June 2017; pp. 63–69.
10. Mastromauro, R.A.; Liserre, M.; Dell’Aquila, A. Control Issues in Single-Stage Photovoltaic Systems: MPPT, Current and Voltage Control. *IEEE Trans. Ind. Inform.* **2012**, *8*, 241–254. [[CrossRef](#)]
11. Yu, D.; Li, Y.; Zhou, Y.; Shi, X.; Liu, H.; Huo, M. Fuzzy control of photovoltaic MPPT based on current perturbation. In Proceedings of the 2017 IEEE 2nd Advanced Information Technology, Electronic and Automation Control Conference (IAEAC), Chongqing, China, 25–26 March 2017; pp. 1683–1687.
12. Ryan, M.J.; Lorenz, R.D. A synchronous-frame controller for a single-phase sine wave inverter. In Proceedings of the APEC 97—Applied Power Electronics Conference, Atlanta, GA, USA, 27 February 1997; Volume 2, pp. 813–819.
13. Bahrani, B.; Rufer, A.; Kenzelmann, S.; Lopes, L.A.C. Vector Control of Single-Phase Voltage-Source Converters Based on Fictive-Axis Emulation. *IEEE Trans. Ind. Appl.* **2011**, *47*, 831–840. [[CrossRef](#)]

14. Zhang, R.; Cardinal, M.; Szczesny, P.; Dame, M. A grid simulator with control of single-phase power converters in D-Q rotating frame. In Proceedings of the IEEE 33rd Annual Power Electronics Specialist Conference, Cairns, Australia, 23–27 June 2002; Volume 3, pp. 1431–1436.
15. Kim, R.Y.; Choi, S.Y.; Suh, I.Y. Instantaneous control of average power for grid tie inverter using single phase D-Q rotating frame with all pass filter. In Proceedings of the IEEE Industrial Electronics Society Conference, Busan, Korea, 2–6 November 2004; pp. 274–279.
16. Verdelho, P.; Marques, G.D. DC voltage control and stability analysis of PWM-voltage-type reversible rectifiers. *IEEE Trans. Ind. Electr.* **1998**, *45*, 263–273. [[CrossRef](#)]
17. Shen, W.J.; Schroder, S.; Stagge, H.; de Doncker, R.W. Precise modeling and analysis of dq-frame current controller for high power converters with low pulse ratio. In Proceedings of the IEEE Energy Conversion Congress and Exposition, Raleigh, NC, USA, 15–20 September 2012; pp. 61–68.
18. Yim, J.-S.; Sul, S.-K.; Bae, B.-H.; Patel, N.; Hiti, S. Modified Current control schemes for high performance permanent magnet AC drives with low sampling to operation frequency ratio. *IEEE Trans. Ind. Appl.* **2009**, *45*, 763–771. [[CrossRef](#)]
19. Shi, J.; Shen, J.; Qu, B.; She, H.; Tan, Z. High Performance complex controller for high-power converters with low-pulse ratios. In Proceedings of the International Conference on Power Electronics and ECCE Asia, Seoul, Korea, 1–5 June 2015; pp. 2180–2187.
20. Holtz, J.; Quan, J.; Pontt, J.; Rodriguez, J.; Newman, P.; Miranda, H. Design of fast and robust current regulators for high-power drivers based on complex state variables. *IEEE Trans. Ind. Appl.* **2004**, *40*, 1388–1397. [[CrossRef](#)]



© 2017 by the authors. Licensee MDPI, Basel, Switzerland. This article is an open access article distributed under the terms and conditions of the Creative Commons Attribution (CC BY) license (<http://creativecommons.org/licenses/by/4.0/>).